Available online at www.sciencedirect.com
SCIENCE DIRECT®
Journal of Sound and Vibration 279 (2005) 669–686
JOURNAL OF SOUND AND VIBRATION
www.elsevier.com/locate/jsvi

Coherent acoustic wave amplification/damping by wrinkled flames

T. Lieuwen*, Ju Hyeong Cho

School of Aerospace Engineering, Georgia Institute of Technology, Atlanta, GA 30332-0150, USA

Received 4 March 2003; accepted 12 November 2003

Abstract

The objective of this paper is to determine the conditions under which a monochromatic acoustic wave incident upon a wrinkled flame is amplified or damped. Recent experiments and analysis have demonstrated that the wrinkled characteristics of the flame act as a source of damping of coherent acoustic energy. This coherent energy is fed into spectrally broadened, incoherent acoustic oscillations. It is also known, however, that acoustic disturbances generate fluctuations in the flame burning velocity and surface area that amplify the acoustic field. Thus, the overall energy in the coherent field depends upon the relative balance between these competing amplification and damping processes. This paper describes an analysis that incorporates these competing processes to determine the conditions under which either dominates.

The analysis includes such factors as the response of the mass burning rate to acoustic perturbations, the temperature change across the flame, and the geometric complexities of the temporally evolving, wrinkled front. Solutions show that acoustic wave amplification/damping characteristics are controlled by the wavelength of the disturbance, the probability density function of the flame front position and orientation, the incident wave angle, the temperature jump across the flame, and the response of the mass burning rate to acoustic perturbations.

1. Introduction

This paper describes results of an investigation of the interactions between a wrinkled, premixed flame front and plane acoustic waves. Such acoustic wave–flame interactions play important roles in the characteristic unsteadiness of turbulent combustion systems found in most processing, power generating, and propulsion applications. In particular, this work is motivated by the

*Corresponding author. Tel.: +1-404-894-3041; fax: +1-404-894-2760.
E-mail address: tim.lieuwen@aerospace.gatech.edu (T. Lieuwen).

0022-460X/$ - see front matter © 2003 Elsevier Ltd. All rights reserved.
doi:10.1016/j.jsv.2003.11.050

problem of combustion instabilities, which routinely plagues the development of combustion systems in industrial processing [1], solid and liquid rockets [2,3], ramjets [4], afterburners, and land-based gas turbines [5]. They generally occur at frequencies associated with the combustors natural longitudinal, radial, azimuthal, or bulk modes. The instabilities arise from interactions between oscillatory flow and heat release processes in the combustor and are manifested as large amplitude, organized oscillations of the combustor's flow fields. The unsteady heat release generated by the acoustic disturbance adds energy to the acoustic field when it is in phase with the pressure oscillations [6].

The basic problem of acoustic waves impinging upon a turbulent flame is depicted in Fig. 1. Upon reaching the flame front, the incident wave is scattered and potentially amplified because of the significant change in gas properties at the flame front and the response of the flame front position and mass burning rate to the perturbations.

Understanding the role of the myriad of processes involved in acoustic–flame interactions requires a fundamental understanding of several sub-problems, many of which have been considered previously. First, because the flame's position and orientation depends upon the local burning rate and flow characteristics, acoustic velocity perturbations cause wrinkling and movement of the flame front. These disturbances have been visualized in several experimental investigations, such as those of DuCruix et al. [7] in a simple Bunsen flame and Shih et al. [8] in a more complex, swirling flow. In addition, calculations of the flame's dynamics and its resultant heat release disturbances have been reported by Boyer and Quinard [9], Fleifil et al. [10], Marble and Candel [11], and Yang and Culick [12]. These studies predict the dependence of the flame's

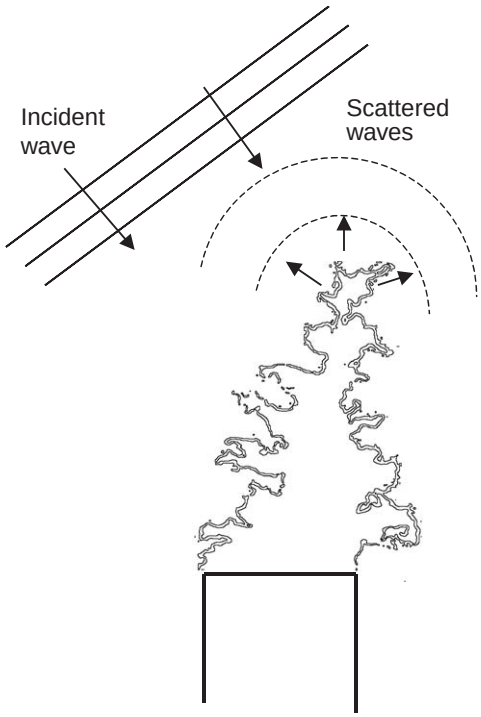

Fig. 1. Instantaneous flame front location in a turbulent flow field (illustration adapted from Dinkelacker et al. [29]).

unsteady heat release upon such parameters as the mean flame position, frequency of oscillations, and mean flow velocity.

Second, the flame burning velocity is sensitive to the perturbations in pressure, temperature, and strain rate that accompany the acoustic wave. McIntosh [13,14], Peters and Ludford [15], and Ledder and Kapila [16], have reported calculations of the unsteady flame structure and determined the transfer function relating the response of the unsteady mass burning rate to pressure fluctuations. The response of the mass burning rate to strain rate fluctuations has been studied analytically by Joulin [17] and computationally by Im and Chen [18].

Third, acoustic, entropy and vorticity modes become strongly coupled at the flame front, leading to energy transfer between these different disturbance modes and amplification or damping of acoustic waves. Calculations of this energy transfer have been reported by Lieuwen [19] and Markstein [20].

Fourth, acoustic waves interact with intrinsic flame instabilities and/or cause parametric flame–acoustic instabilities. The parametric acoustic instability of planar flames is due to the periodic acceleration of the flame front by the unsteady flow field, which separates two regions of differing densities. Such instabilities are often observed in flames as they propagate toward the open end of a tube and have been investigated in several experimental [20,21] and theoretical investigations [22,23]. In addition, it has been shown that acoustic oscillations can stabilize the Darrieus–Landau flame instability [21].

The majority of the literature addressing this problem focuses on the acoustic wave–laminar flame interaction problem. More limited attention has been given to the interactions between acoustic waves and turbulent flames with temporally evolving, convoluted, and multi-connected fronts. Some aspects of this problem have been addressed in recent work of the authors, who analyzed wave scattering from wrinkled flame fronts by modelling the flame as a dynamically evolving, corrugated discontinuity whose local burning velocity is a function of the instantaneous acoustic field [24,25]. This paper extends this work to determine the conditions under which waves are amplified or damped as they interact with a wrinkled flame.

The authors' prior work [24,25] suggests that several qualitative differences exist between the characteristics of waves scattered from laminar and turbulent flames. In order to motivate the work reported here, the principal results of these studies are summarized below. The result of most relevance to this study is the prediction that a coherent, harmonically oscillating acoustic wave, p'_{drive}, incident upon a turbulent flame generates both coherent, $p'_{s,c}$, and incoherent, $p'_{s,i}$, scattered waves. The dynamic, wrinkled characteristics of turbulent flames decrease the energy in the coherent acoustic field by transferring it to the incoherent field. As such, the power in the scattered coherent and incoherent fields decreases and increases, respectively, as the scale of flame wrinkling, σ, increases and/or the acoustic wavelength, λ, decreases. This coherent energy damping source is particularly significant for disturbances whose wavelengths are on the order of the characteristic scales of flame wrinkling, i.e., $\sigma/\lambda \sim O(1)$. At small σ/λ values, it predicts that the incoherent scattered power increases exponentially with σ/λ. Its dependence upon σ/λ saturates for large σ/λ, however, as its upper limit is constrained by the power in the incident field.

The random movement of the flame front serves as the mechanism for this coherent to incoherent field energy transfer. It causes the scattered field to oscillate over a range of Doppler shifted frequencies from that of the incident wave. It has been shown that the incoherent field frequency spectrum has sidebands about the frequency of the incident wave whose spectral

characteristics are a function of the flame front movement spectrum, i.e., $p_{s,i}(f) = g(\zeta(f - f_{drive}))$, where $p_{s,i}(f)$, $\zeta(f)$ and f_{drive} denote the power spectra of the scattered incoherent acoustic field, the power spectra of the flame front position, and the frequency of the incident wave, respectively. The basic characteristics of these distributed sidebands can be understood from the following considerations. A stationary source generates a harmonically oscillating acoustic wave that is incident upon a surface moving with a Mach number of **M**. A stationary observer will measure the reflected wave oscillating at the Doppler shifted frequency

$$f_{refl} = f_{drive}(1 + 2\mathbf{M} \cdot \mathbf{n}), \quad (\mathbf{M} \cdot \mathbf{n} \ll 1) \tag{1}$$

where **n** denotes the unit normal direction of the incident wave. This expression shows that the spectral bandwidth of the reflected waves is given by

$$\langle (f - f_{drive})^2 \rangle^{1/2} = \langle (\Delta f)^2 \rangle^{1/2} \approx 2 f_{drive} \langle (\mathbf{M} \cdot \mathbf{n})^2 \rangle^{1/2}. \tag{2}$$

These results suggest that acoustic interactions with turbulent flames result in narrow band noise generation whose bandwidth is determined by that of the flame front movement and center frequency by that of the incident wave. It should be pointed out, however, that the above argument does not account for surface wrinkling and, thus, is most relevant to the $\sigma/\lambda \ll 1$ case.

Several fundamental predictions of this theory have been confirmed in acoustic scattering measurements [26] which are presented next. Fig. 2 plots a detail of the measured spectrum when $f_{drive} = 7.5$ kHz for the cases where the flame is on and transducer off, transducer is on and flame off, and both flame and transducer are on. Note the narrow bandwidth of the acoustic spectra when only the transducer is on. When the transducer and flame are both on, the acoustic spectrum has substantially higher values than the background combustion noise in the frequency interval centered around the driving frequency. For example, at $f = 7.51$ kHz, it is two orders of magnitude higher than the background combustion noise. In this case, the scattered acoustic waves can be distinguished from background noise over a bandwidth of about 100 Hz.

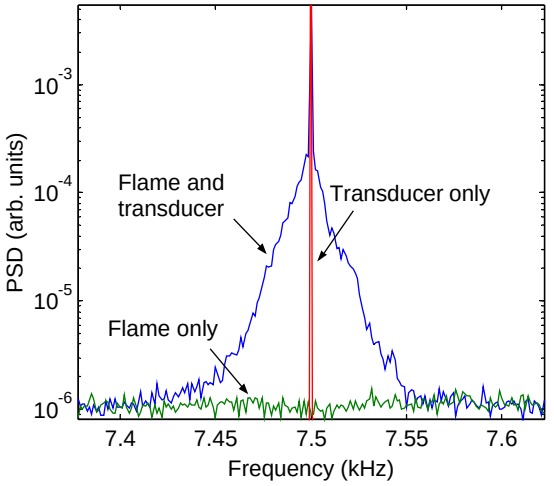

Fig. 2. Acoustic spectra measured with only the flame on, only the transducer is on, and both on showing distributed sidebands about driving frequency.

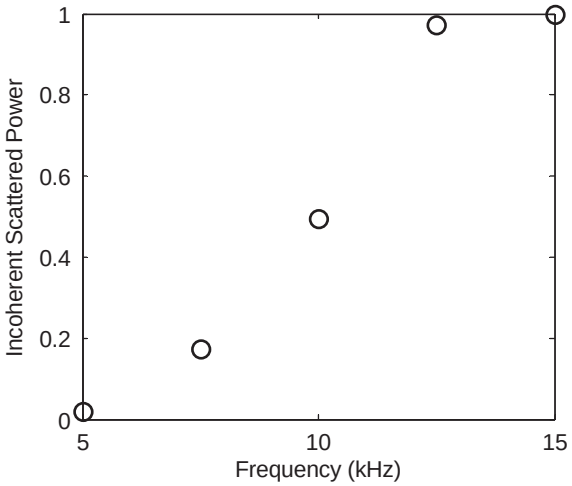

Fig. 3. Dependence of total power in scattered incoherent field, normalized by its value at 15 kHz, upon driving frequency.

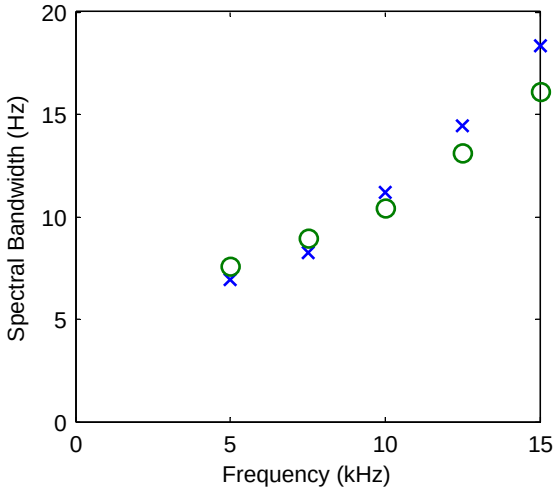

Fig. 4. Dependence of spectral bandwidth of scattered acoustic field upon incident wave frequency ($\times, \phi = 0.93$; $\bigcirc$, $\phi = 0.79$).

Fig. 3 plots the dependence of the scattered power in the incoherent sidebands upon the driving frequency. It shows that the scattered power increases substantially at lower frequencies, and then appears to saturate to a limiting value. This result is in good agreement with the discussion above. Finally, Fig. 4 plots the dependence of the spectral bandwidth upon driving frequency. In agreement with the Doppler shift arguments above, the figure shows that it monotonically increases with driving frequency.

The above experimental results clearly demonstrate the key predictions of the theory—that coherent acoustic energy is transferred into the incoherent field. Our objective in this paper is to

further pursue this observation—in particular, to quantify the conditions under which the competing amplification (by burning velocity perturbations) and damping (by transfer to incoherent oscillations) processes dominate and, thereby, to determine when the coherent field is amplified or damped as a result of the interaction.

2. Analysis

The geometry under consideration is the same as prior analyses [24,25] and consists of a time varying, wrinkled flame surface, see Fig. 5. The average position of the flame is flat and its instantaneous position is given by $\zeta(x, y, t)$. Since the basic modelling approach has been detailed elsewhere [24,25], we only summarize its basic assumptions and principle results. These assumptions are: (1) flame thickness is much smaller than an acoustic wavelength, (2) outside of the flame, the flow field is isothermal, has a low Mach number, M, and is composed of a perfect gas; as such, convective affects (e.g., wave scattering by turbulent flow fluctuations) on wave propagation are neglected, (3) the acoustic field can be approximately described with the single scattering Kirchoff approximation. The Kirchoff approximation assumes that the pressure–velocity relation (i.e., the impedance) of the wave at each point along the flame front is equal to its flat surface value at those local conditions. In this case, the flame front locally "looks" planar to the incident acoustic wave. More detailed analyses show that this approximation is accurate when [27]

$$\frac{k_j \sigma \cos^3 \theta_j}{\sigma_\Delta^2} \gg 1, \qquad \sigma_\Delta^2 \tan^2 \theta_j \ll 1, \tag{3,4}$$

where the subscript j has a value of one or two, depending upon whether the wave field up or downstream of the flame is being considered. The first condition roughly states that the acoustic wavelength in the burned and unburned gases must be much smaller than the mean squared radius of curvature of the flame front. The second shows that the mean squared slope of the flame

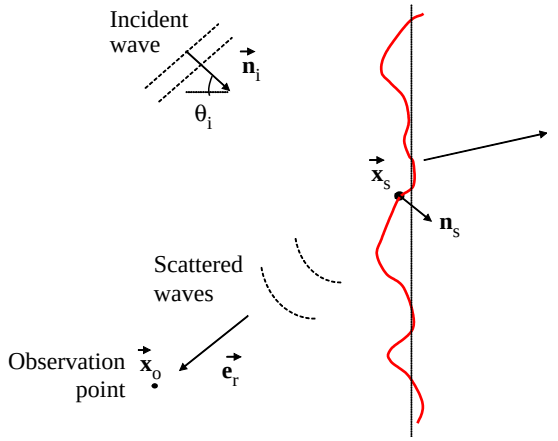

Fig. 5. Schematic illustrating flame surface and acoustic field quantities.

front must be small relative to that of the incident wave to minimize "shadowing" and multiple reflections.

The reflection coefficient (or impedance) at each point along the flame front can be determined from laminar flame analyses, such as described in Ref. [13]. The specific result depends upon the model for the flame's response to acoustic perturbations. Below, we use McIntosh's result [13] that relates the local flame speed perturbation to the acoustic pressure at the flame to yield

$$V(\mathbf{x}_s,t)=\frac{(\bar{\rho}_2\bar{c}_2/\bar{\rho}_1\bar{c}_1)(\mathbf{n}_i\cdot\mathbf{n}_s)+\gamma\kappa-\sqrt{1-(\bar{c}_2/\bar{c}_1)^2(1-(\mathbf{n}_i\cdot\mathbf{n}_s)^2)}}{(\bar{\rho}_2\bar{c}_2/\bar{\rho}_1\bar{c}_1)(\mathbf{n}_i\cdot\mathbf{n}_s)-\gamma\kappa+\sqrt{1-(\bar{c}_2/\bar{c}_1)^2(1-(\mathbf{n}_i\cdot\mathbf{n}_s)^2)}}. \tag{5}$$

As such, the analysis restricts its attention to pressure-coupled flame response mechanisms. Although not necessary to proceed with the analysis, we neglect changes in molecular weight, specific heats ratio, and mean pressure of the gases across the flame, so that the density and sound speed ratios are related to the temperature ratio across the flame as $\bar{\rho}_2\bar{c}_2/\bar{\rho}_1\bar{c}_1=\sqrt{1/\Lambda}$ and $\bar{c}_2/\bar{c}_1=\sqrt{\Lambda}$. The coefficient κ quantifies the flame speed response to acoustic perturbations and is given by

$$\kappa=\frac{2M_s\Theta(\tilde{\Lambda}-1)(\gamma-1)}{\gamma\sqrt{\tilde{\Lambda}}}\frac{(-\mathrm{i}\omega\tau)(s-1+1/\tilde{\Lambda})}{(\Theta(\tilde{\Lambda}-1)/\tilde{\Lambda})[Le(s-1)+(1-r)]-2s(1-r)}, \tag{6}$$

where τ is a characteristic flame diffusion time, Le is the Lewis number, $s=\sqrt{1-4\mathrm{i}\omega\tau/Le}$, $r=\sqrt{1-4\mathrm{i}\omega\tau}$, and $\tilde{\Lambda}=T_{burned}/T_{unburned}$ (note that Λ equals $T_{burned}/T_{unburned}$ or $T_{unburned}/T_{burned}$ if the incident wave originates from up or downstream of the flame, respectively). Typical κ values fall in the 10^{-3}–10^{-1} range. It increases roughly linearly with activation energy, Θ, and as $\sqrt{\omega}$ and $\sqrt{\tilde{\Lambda}}$. The Lewis number dependence is weak for $Le\sim1$.

We next focus on the reflected and transmitted coherent field solutions. Although not necessary to proceed with the analysis, to simplify the results we assume that the statistical characteristics of the flame front are spatially uniform and that the statistics of the local flame front position, ζ and slope, $\nabla\zeta$, are independent. The solutions are then given by [24]

$$\frac{\langle p_R\rangle}{p'_{R,lam}}=\frac{w_R\langle R\rangle}{R_{\varsigma=0}},\qquad \frac{\langle p_T\rangle}{p'_{T,lam}}=\frac{w_T\langle T\rangle}{T_{\varsigma=0}}, \tag{7,8}$$

where the subscripts R and T denote the reflected and transmitted value and p'_{lam} denotes the pressure in the case where the flame front is smooth (i.e., $\zeta=0$). These quantities are given by [24]

$$w_R=\int_{-\infty}^{\infty}B(\varsigma)\mathrm{e}^{-2\mathrm{i}k_1\varsigma\cos\theta_i}\,\mathrm{d}\varsigma,\qquad w_T=\int_{-\infty}^{\infty}B(\varsigma)\mathrm{e}^{-\mathrm{i}k_1\left(\cos\theta_i-\sqrt{1/\Lambda-\sin^2\theta_i}\right)\varsigma}\,\mathrm{d}\varsigma, \tag{9,10}$$

$$R=\frac{(\varsigma_x\sin\theta_i+\cos\theta_i)+\gamma\kappa\sqrt{\Lambda(1+|\nabla\varsigma|^2)}-\sqrt{\Lambda(1-\Lambda)(1+|\nabla\varsigma|^2)+\Lambda^2(\varsigma_x\sin\theta_i+\cos\theta_i)^2}}{(\varsigma_x\sin\theta_i+\cos\theta_i)-\gamma\kappa\sqrt{\Lambda(1+|\nabla\varsigma|^2)}+\sqrt{\Lambda(1-\Lambda)(1+|\nabla\varsigma|^2)+\Lambda^2(\varsigma_x\sin\theta_i+\cos\theta_i)^2}}, \tag{11}$$

$$T=\frac{(1-R)(\varsigma_x\sin\theta_i+\cos\theta_i)+(1+R)\left(\Lambda\varsigma_x\sin\theta_i+\sqrt{\Lambda(1-\Lambda\sin^2\theta_i)}\right)}{2\sqrt{\Lambda(1-\Lambda\sin^2\theta_i)}}, \tag{12}$$

$$\langle R\rangle = \int_{-\infty}^{\infty}\int_{-\infty}^{\infty} B(\varsigma_x,\varsigma_y)R\,\mathrm{d}\varsigma_x\,\mathrm{d}\varsigma_y, \qquad \langle T\rangle = \int_{-\infty}^{\infty}\int_{-\infty}^{\infty} B(\varsigma_x,\varsigma_y)T\,\mathrm{d}\varsigma_x\,\mathrm{d}\varsigma_y. \tag{13, 14}$$

$B(\zeta)$ and $B(\zeta_x,\zeta_y)$ are the probability density functions (PDF) of the flame front position and gradient, respectively. Note that, with a change of co-ordinates, the PDF $B(\zeta_x,\zeta_y)$ is identical to the flame surface normal PDFs measured by Gouldin and co-workers [28].

Finally, the ratio of the net flux of energy out of the flame, normalized by that of the incident wave is

$$\Pi = |\langle R\rangle^2|w_R^2 + \frac{\sqrt{\Lambda(1-\Lambda\sin^2\theta_i)}}{\cos\theta_i}|\langle T\rangle^2|w_T^2 - 1. \tag{15}$$

This quantity is identically zero if no coherent acoustic energy is produced by the flame. It is positive or negative if the coherent field is amplified or damped, respectively.

Eq. (7) shows that the characteristics of the scattered field depends upon the product of two quantities, w_R and $\langle R\rangle$. The quantity w_R depends only upon the flame surface position and reflects purely kinematic processes; i.e., the phase of the reflected wave differs from point to point along the flame front because of differences in distance the wave travels before impinging upon the flame and reflecting. If the flame position is symmetric about its mean (i.e., all odd statistical moments of ζ are zero), then w_R and w_T are real, implying that the phase of the coherent field in the wrinkled flame case is the same as in the flat flame case. If the flame position is asymmetric, then the phase of the coherent field is offset from its smooth surface value.

In contrast, the quantities $\langle R\rangle$ and $\langle T\rangle$ depend only upon the flame position gradient; they represent the "average" reflection and transmission coefficients of the flame. They contain the mass burning rate response term and the dependence of the surface reflection coefficient upon the relative angle between the wave and flame surface.

3. Results and discussion

Eqs. (9)–(15) are general results describing the characteristics of the coherent scattered acoustic field in terms of the statistical characteristics of the flame position $B(\zeta)$ and its spatial gradient, $B(\zeta_x,\zeta_y)$, the angle of the incident wave, θ_i, the wave number of the disturbance, k, the temperature ratio across the flame, Λ, and the burning rate response parameter, κ. This section presents typical results explicitly illustrating these dependencies for a two-dimensional surface, i.e., $\zeta = \zeta(x,t)$

Explicitly evaluating the quantities of interest requires specifying flame front position and gradient PDFs, $B(\zeta)$ and $B(\zeta_x)$. We use a Gaussian PDF for $B(\zeta)$ and a clipped Gaussian for $B(\zeta_x)$ (a clipped Gaussian PDF is used to avoid large gradients where the developed theory is not applicable):

$$\zeta_x < 5\sigma_\Delta\text{: } B(\zeta_x) = C\mathrm{e}^{-\zeta_x^2/2\sigma_\Delta^2}, \tag{16}$$

$$\zeta_x > 5\sigma_\Delta\text{: } B(\zeta_x) = 0, \tag{17}$$

where $\sigma_\Delta^2 = \langle |\nabla\zeta|^2 \rangle$ and C denotes the variance of the surface gradient and normalizing constant, respectively. This assumed gradient PDF is quite similar in shape to those measured by Gouldin's group [28] where they measure σ_Δ values of 0.3–0.4. The author is not aware of any published position PDF measurements, $B(\zeta)$.

The integrals in Eqs. (9)–(10) can be evaluated explicitly:

$$w_R = e^{-2(k_1\sigma\cos\theta_i)^2}, \qquad w_T = e^{-\left(k_1\sigma\left(\cos\theta_i - \sqrt{1/\Lambda - \sin^2\theta_i}\right)\right)^2/2}, \tag{18, 19}$$

where σ^2 is the mean squared deviation of the flame from its average position, $\sigma^2 = \langle \zeta^2 \rangle$. It is a measure of the flame brush thickness. Plots illustrating the typical dependence of w_R and w_T upon $k\sigma$ are shown in Fig. 6. The figure shows that they decay rapidly with increasing $k\sigma = 2\pi\sigma/\lambda$.

Determination of $\langle R \rangle$ and $\langle T \rangle$ requires numerical integration of Eqs. (13)–(14). Discussion of the dependence of $\langle R \rangle$ and $\langle T \rangle$ upon θ_i, Λ, and κ have been published elsewhere [25], so only limited results are presented here. As illustrated in Fig. 7, $\langle R \rangle$ exhibits a strong dependence upon

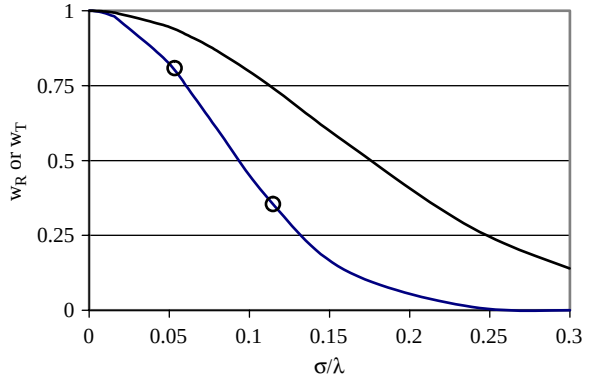

Fig. 6. Dependence of kinematic reflection and transmission parameters w_R (O) and w_T (-) upon ratio of flame brush thickness, σ, to acoustic wavelength, λ (based upon sound speed in cold gas; $\theta_i = 30$, $\Lambda = 0.25$).

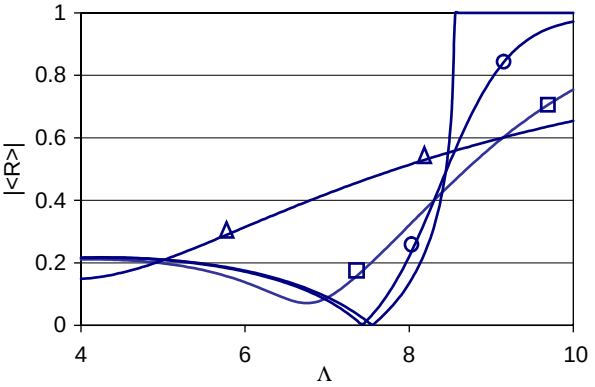

Fig. 7. Amplitude dependence of the wrinkled flame reflection coefficient, $\langle R \rangle$, upon the temperature ratio across the flame, Λ, for $\sigma_\Delta = 0$ (−), 0.01 (O), 0.03 (□), and 0.1 (Δ) ($\theta_i = 20^\circ$, $\kappa = 0$).

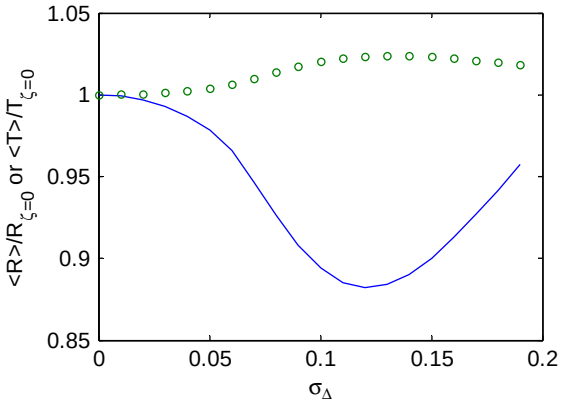

Fig. 8. Dependence of average reflection (-) and transmission (o) coefficient upon flame slope parameter ($M_s = 0.001$, $\gamma = 1.4$, $\Theta = 15$, $Le = 1$, $2\pi\omega\tau = 10$, $\Lambda = 8$, $\theta_i = 10^\circ$).

Λ if the wave is incident from the reactants side (i.e., $\Lambda > 1$) in the smooth flame case, $\sigma_\Delta = 0$. In particular, at incident angles greater than $\sin^{-1}(1/\sqrt{\Lambda})$ (the cut-off angle), no energy is transmitted and the wave is completely reflected. This behavior is analogous to that occurring in other wave propagation phenomenon when a disturbance propagating in a lower sound speed medium impinges upon a higher sound speed region. This dependence is smoothed out substantially with increasing σ_Δ.

For incident angles below the cut-off value, changes in $\langle R \rangle$ are largely compensated by corresponding changes in $\langle T \rangle$, as illustrated in Fig. 8. The figure plots the dependence of $\langle R \rangle$ and $\langle T \rangle$, normalized by their smooth front results, upon σ_Δ. It shows that these quantities exhibit opposite dependence upon σ_Δ. Consequently, the overall effect of variations in σ_Δ appears to be a modification of the average reflection and transmission coefficients, but with little overall effect on the energy that is produced/damped by the interaction; see the curve labelled $\theta_i = 10^\circ$ in Fig. 9. The parameter σ_Δ does have an effect upon the overall energy balance if the wave is incident at angles above cutoff so that the transmission coefficient is identically zero. In this case, its effect upon $\langle R \rangle$ directly effects Π, as can be seen in the $\theta_i = 22^\circ$ curve in Fig. 9.

We next consider characteristics of the overall coherent acoustic energy produced or damped by the flame, Π, in more detail. The rest of this section presents typical results illustrating the dependence of Π upon θ_i, σ/λ, $\omega\tau$, and σ_Δ. Note that variation of the parameter σ/λ implies either changes in flame brush thickness, σ, at a fixed wavelength, or variation of wavelength for a fixed flame brush. Results below were obtained for both situations. In the former case, the flame response characteristics remain constant, so that increases in σ/λ results in an exponential reduction of the coherent field amplitude as described by Eqs. (18)–(19). In the latter case, increases in σ/λ imply an increase in frequency (i.e., a reduction in wavelength). Since the flame response increases with frequency, the overall coherent field balance becomes more complex because of the competing effects of flame response (increases with frequency) and coherent field damping (also increases with frequency). Since the driving process increases as $\sqrt{f}$ and damping as e^{-f^2}, the damping processes dominate at high frequencies.

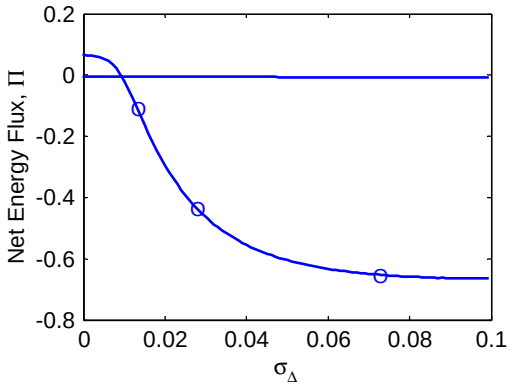

Fig. 9. Dependence of net energy flux upon flame slope parameter for $\theta_i = 10^\circ$ (-) and 22° (O) ($M_s = 0.001$, $\gamma = 1.4$, $\Theta = 15$, $Le = 1$, $2\pi\omega\tau = 10$, $\Lambda = 8$, $\sigma/\lambda = 0.016$, where λ is wavelength in unreacted gas).

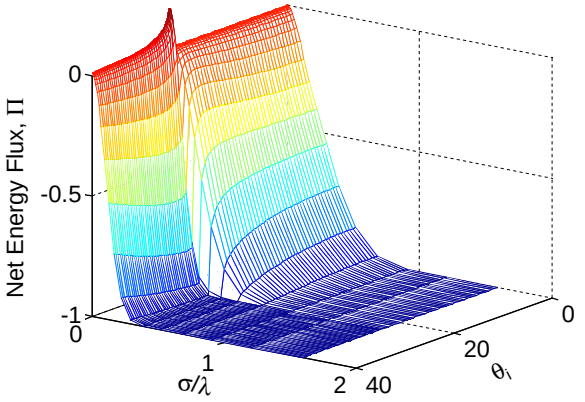

Fig. 10. Dependence of net energy flux, Π, upon dimensionless ratio of wrinkled flame brush thickness to acoustic wavelength (in the cold gas), σ/λ, and angle of incidence, θ_i. Wave incident from upstream ($M_s = 0.001$, $\gamma = 1.4$, $Le = 1$, $\Theta = 15$, $\Lambda = 6$, $2\pi\omega\tau = 10$).

Figs. 10 and 11 plot the dependence of Π upon σ/λ and θ_i for a wave incident from upstream. This baseline result was obtained for $\sigma_\Delta = 0$. The results illustrate that Π has values exceeding zero (implying wave amplification) for low σ/λ values, but rapidly decreases to a value of -1 (implying 100% damping of incident coherent energy). Note the discontinuous behavior of the solution at the cut-off angle, $\theta_i \sim 25^\circ$. At angles above this value, no coherent energy is transmitted through the flame and total reflection occurs. As such, the overall coherent field damping discontinuously increases, because of the shorter wavelengths in the cold, unreacted region. Fig. 12 plots an analogous result for the case where the wave is incident from downstream. The figure shows that Π exhibits little dependence upon the angle of incidence in this case. The overall characteristics of Π are qualitatively similar for other cases. The rest of the results presented use contour plots with a single line that demarcates the parameter regimes where waves are amplified or damped.

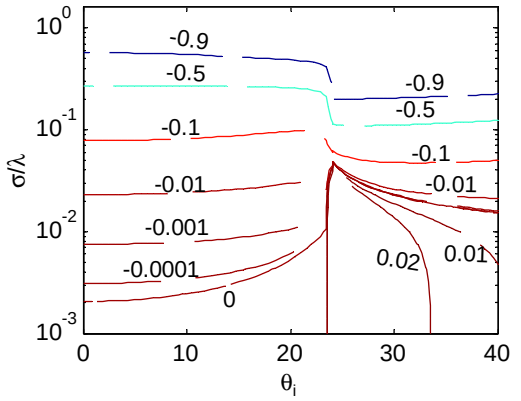

Fig. 11. Contour plot of constant energy flux values; same results as plotted in Fig. 10.

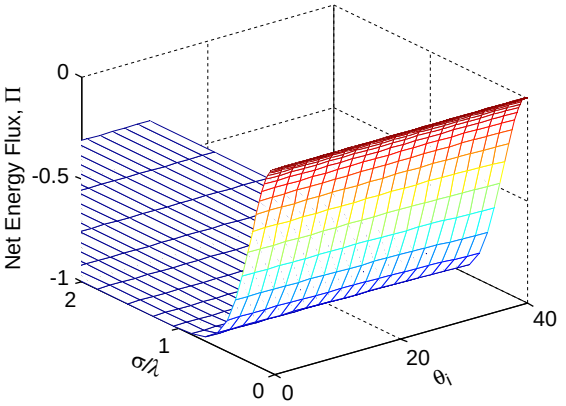

Fig. 12. Dependence of net energy flux, Π, upon dimensionless ratio of wrinkled flame brush thickness to acoustic wavelength (in the cold gas), σ/λ, and angle of incidence, θ_i. Wave incident from downstream ($M_s = 0.001$, $\gamma = 1.4$, $Le = 1$, $\Theta = 15$, $\Lambda = \frac{1}{6}$, $2\pi\omega\tau = 10$).

Introducing finite values of σ_Δ places limitations on the parameter regime where the developed theory is valid, as can be seen from Eqs. (3)–(4). The contour plots below block out these regions where the theory cannot be applied. It is assumed that the inequality is satisfied if the left side exceeds the right by a factor of 10. For example, Fig. 13 shows two regions blocked out. The region stretching from $\theta_i = 0$–40° for low values of σ/λ reflects the limitations on the theory on the unreacted side of the flame. The theory is inaccurate in the hot, reacted side in the region stretching from $\theta_i = 15$–25° for almost all σ/λ values. This region extends to much larger σ/λ values because the transmitted field propagates nearly parallel to the flame front, i.e., $\theta_T \sim 90^\circ$, in the vicinity of the cut-off angle.

Consider first the case of fixed σ, but varying λ. Fig. 13 plots the dependence of the $\Pi = 0$ contour upon σ/λ and θ_i. The region below the line corresponds to the $\Pi > 0$, wave amplification region. Results are presented at four values of the dimensionless ratio of flame brush thickness to

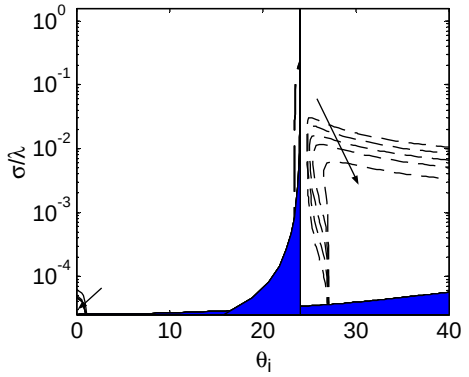

Fig. 13. Dependence of net energy flux = 0, $\Pi = 0$, contour upon dimensionless ratio of wrinkled flame brush thickness to acoustic wavelength (in the cold gas), σ/λ, and angle of incidence, θ_i. Results obtained at values of $\sigma/\delta = 5$, 10, 20, 40, and 100 (arrow points in direction of increasing σ/δ). Wave incident from upstream. Theory not applicable in shaded areas ($M_s = 0.001$, $\gamma = 1.4$, $Le = 1$, $\Theta = 15$, $\Lambda = 6$, $2\pi\omega\tau = 10$, $\sigma_\Delta = 0.004$).

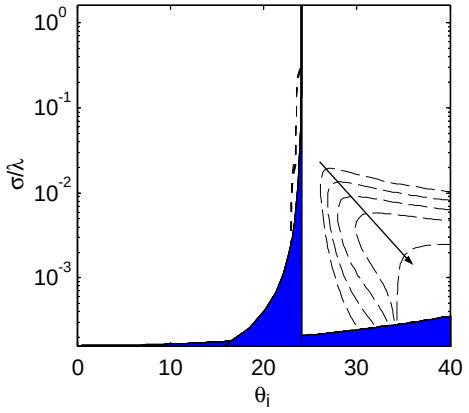

Fig. 14. Same result as in Fig. 13 but flame gradient parameter $\sigma_\Delta = 0.01$. Results obtained at values of $\sigma/\delta = 5$, 10, 20, 40, and 100 (arrow points in direction of increasing σ/δ).

flame thickness, $\sigma/\delta = 2\pi(\sigma/\lambda)(1/\omega\tau)$. The arrows in the figure point in the direction of increasing σ/δ. The figure shows that a large region of amplification occurs for $\theta_i > 25$ and a much smaller one for $\theta_i < 5$. The accuracy of the amplification region indicated on the figure in the $\theta_i \sim 25$ region is questionable, however, due to its proximity to the shaded region where the theory is not valid.

Fig. 14 plots a similar result where σ_Δ has a value of 0.01. As can be anticipated from the above discussion, the amplification regions for incident angles above cutoff are smaller than in Fig. 13. Similar results are plotted for the downstream incidence case in Figs. 15 and 16. Fig. 17 illustrates a similar result as in the above two plots, but with σ_Δ increased to 0.01. Since there is no cut-off phenomenon in this situation, the size of the amplification regions do not substantially change. This result can be anticipated from the above discussion; e.g., see Fig. 9.

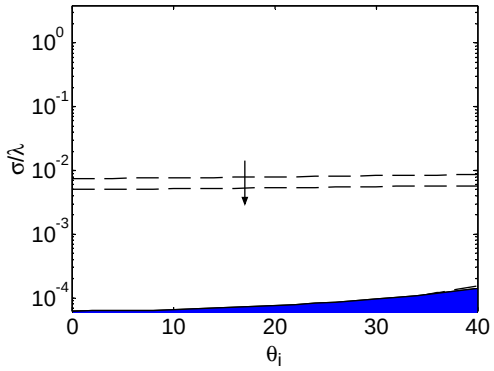

Fig. 15. Same results as in Fig. 13, but wave incident from downstream. Results obtained at values of $\sigma/\delta = 5$ and 7.5 (arrow points in direction of increasing σ/δ).

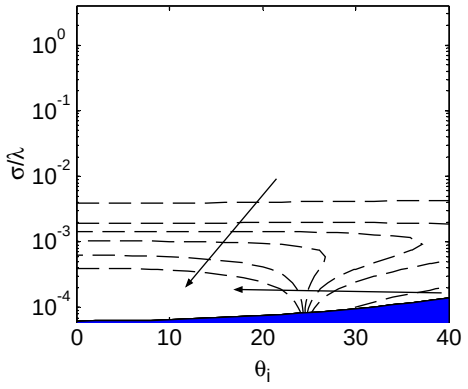

Fig. 16. Same results as in Fig. 13, but wave incident from downstream. Results obtained at values of $\sigma/\delta = 10$, 20, 25, 30, 40, 500 (arrow points in direction of increasing σ/δ).

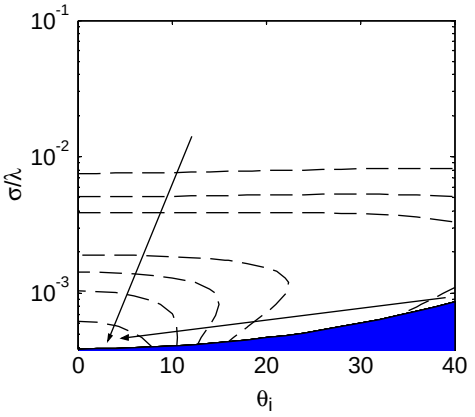

Fig. 17. Same results as in Fig. 16, but flame gradient parameter $\sigma_{\Delta} = 0.01$. Results obtained at values of $\sigma/\delta = 5$, 7.5, 10, 20, 25, 30, and 40 (arrow points in direction of increasing σ/δ).

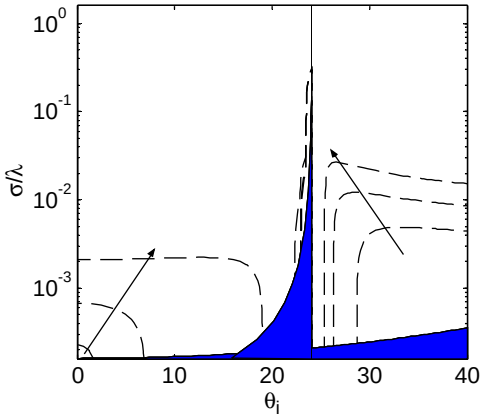

Fig. 18. Dependence of net energy flux $= 0$, $\Pi = 0$, contour upon dimensionless ratio of wrinkled flame brush thickness to acoustic wavelength (in the cold gas), σ/λ, and angle of incidence, θ_i. Results obtained at values of $2\pi\omega\tau = 0.1$, 1, and 10 (arrow points in direction of increasing $2\pi\omega\tau$). Wave incident from upstream. Theory not applicable in shaded areas ($M_s = 0.001$, $\gamma = 1.4$, $Le = 1$, $\Theta = 15$, $\Lambda = 6$, $\sigma_\Delta = 0.01$).

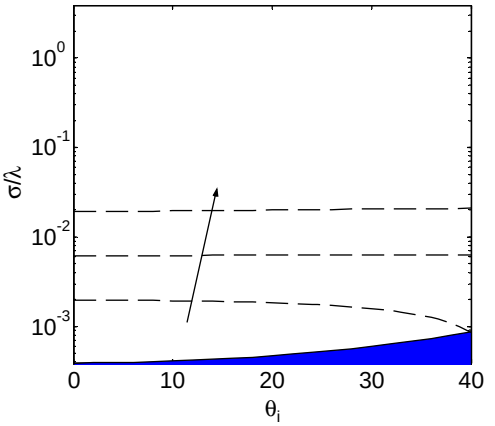

Fig. 19. Same result as in Fig. 18, but wave incident from downstream ($\Lambda = \frac{1}{6}$).

We next consider the case of fixed f but varying σ. Fig. 18 illustrates similar results as in the above contour plots, where the three $\Pi = 0$ lines were calculated at different frequencies. As expected, the regions of amplification increase with frequency. Fig. 19 plots a comparable result, but where the incident wave originates from downstream.

In order to obtain a feel for actual numbers, consider the case of a stoichiometric methane/air flame. A $2\pi\omega\tau = 1$ value roughly corresponds to a frequency of $f = 400$ Hz. Fig. 18 indicates that waves are amplified for σ/λ values of less than 10^{-2} in the $\theta_i \sim 27$–40° region. Assuming an unreacted gas temperature of 300 K implies wave amplification for flame brush thicknesses less than 1 cm.

4. Concluding remarks

The above results show that incorporating flame wrinkling effects sharply reduces the regions where pressure-coupled flame response amplifies acoustic disturbances. For cases where the wave is incident either from downstream, or from upstream at angles below cutoff, the regions of amplification have little dependence upon σ_Δ values. Amplification regions shrink with increases in σ_Δ for waves incident above the cut-off value. In either case, the parameter does significantly effect the relative balance of acoustic energy that is reflected and transmitted. Also, the amplification regions have little and substantial dependence upon θ_i for waves incident from up/downstream of the flame, respectively.

Acknowledgements

This research was supported by the National Science Foundation under contract CTS-0122578 (Dr. Farley Fisher, technical monitor).

Appendix A. Nomenclature

B probability density function
c sound speed
f frequency
k wave number, ω/c
m mass burning rate
M_s flame speed Mach number relative to unburned gas
p pressure
R reflection coefficient
T transmission coefficient
V reflection coefficient
w_R defined in Eq. (9)
w_T defined in Eq. (10)

Greek letters

δ laminar flame thickness
γ ratio of specific heats
κ mass burning rate sensitivity to pressure perturbations
λ acoustic wavelength
ρ density
σ^2 variance of flame front position, $\langle \zeta^2 \rangle$
σ_Δ^2 variance of flame front gradient, $\langle |\nabla \zeta|^2 \rangle$
θ_i incident plane wave angle
Θ dimensionless activation energy, E_a/RT_{burned}

τ characteristic flame diffusion time
ω angular frequency
ζ flame position, see Fig. 5
Λ temperature ratio across flame, T_2/T_1

Subscripts/superscripts

($'$) fluctuating quantity
($^-$) mean quantity
i incident wave
lam laminar flame value
1 variable's value on side of flame which wave originates from
2 variable's value on opposite side of flame from which wave originates

References

[1] A. Putnam, *Combustion Driven Oscillations in Industry*, American Elsevier Publishers, New York, 1971.
[2] E.W. Price, Combustion instability in solid propellant rocket motors, *Astronautica Acta* 5 (1959) 63–72.
[3] L. Crocco, S. Cheng, *Theory of Combustion Instability in Liquid Propellant Rocket Motors*, Butterworths Scientific Publications, London, 1956.
[4] U.G. Hegde, D. Reuter, B.R. Daniel, B.T. Zinn, Flame driving of longitudinal instabilities in dump type Ramjet combustors, *Combustion Science and Technology* 55 (1987) 125–138.
[5] A.A. Peracchio, W.M. Proscia, Nonlinear heat release/acoustic model for thermo-acoustic instability in lean premixed combustors, *Journal of Engineering for Gas Turbines & Power* 121 (1999) 415–421.
[6] J.S.W. Rayleigh, *The Theory of Sound*, Vol. 2, Dover, New York, 1945, p. 226.
[7] S. DuCruix, D. Durox, S. Candel, Theoretical and experimental determinations of the transfer function of a laminar premixed flame, *Proceedings of the Combustion Institute* 28 (2000) 765–773.
[8] W.P. Shih, J. Lee, D. Santavicca, Stability and emissions characteristics of a lean premixed gas turbine combustor, *Proceedings of the Combustion Institute* 26 (1996) 2771–2778.
[9] L. Boyer, J. Quinard, On the dynamics of anchored flames, *Combustion and Flame* 82 (1990) 51–65.
[10] M. Fleifil, A.M. Annaswamy, Z.A. Ghoniem, A.F. Ghoniem, Response of a laminar premixed flame to flow oscillations: a kinematic model and thermoacoustic instability results, *Combustion and Flame* 106 (1996) 487–510.
[11] F.E. Marble, S.M. Candel, An analytical study of the non-steady behavior of large combustors, *Proceedings of the Combustion Institute* 17 (1978) 761–769.
[12] V. Yang, F.E.C. Culick, Analysis of low frequency combustion instabilities in a laboratory Ramjet combustor, *Combustion Science and Technology* 45 (1986) 1–25.
[13] A.C. McIntosh, Pressure disturbances of different length scales interacting with conventional flames, *Combustion Science and Technology* 75 (1991) 287–309.
[14] A.C. McIntosh, Deflagration fronts and compressibility, *Philosophical Transactions of the Royal Society of London* 357 (1999) 3523–3538.
[15] N. Peters, G.S.S. Ludford, The effect of pressure variations on premixed flames, *Combustion Science and Technology* 34 (1983) 331–344.
[16] G. Ledder, A.K. Kapila, The response of premixed flames to pressure perturbations, *Combustion Science and Technology* 76 (1991) 21–44.
[17] G. Joulin, On the response of premixed flames to time dependent stretch and curvature, *Combustion Science and Technology* 97 (1994) 219–229.
[18] H.G. Im, J.H. Chen, Effects of flow transients on the burning velocity of laminar hydrogen/air premixed flames, *Proceedings of the Combustion Institute* 28 (2000) 1833–1840.

[19] T. Lieuwen, Theoretical investigation of unsteady flow interactions with a premixed planar flame, *Journal of Fluid Mechanics* 435 (2001) 289–303.
[20] G.H. Markstein (Ed.), *Nonsteady Flame Propagation*, Pergamon Press, Oxford, 1964.
[21] G. Searby, D. Rochwerger, A parametric acoustic instability in premixed flames, *Journal of Fluid Mechanics* 231 (1991) 529–543.
[22] P. Pelce, D. Rochwerger, Vibratory instability of cellular flames propagating in tubes, *Journal of Fluid Mechanics* 239 (1992) 293–307.
[23] P. Clavin, P. Pelce, L. He, One-dimensional vibratory instability of planar flames propagating in tubes, *Journal of Fluid Mechanics* 216 (1990) 299–322.
[24] T. Lieuwen, Theory of high frequency acoustic wave scattering by turbulent flames, *Combustion and Flame* 126 (1–2) (2001) 1489–1505.
[25] T. Lieuwen, Analysis of acoustic wave interactions with turbulent, premixed flames, *Proceedings of the Combustion Institute* 29 (2002) 1817–1824.
[26] T. Lieuwen, Y. Neumeier, R. Rajaram, Measurements of incoherent acoustic wave scattering from turbulent premixed flames, *Proceedings of the Combustion Institute* 29 (2002) 1809–1815.
[27] V. Voronovich, *Wave Scattering from Rough Surfaces*, Springer, New York, 1999.
[28] D.A. Knaus, F.C. Gouldin, *Proceedings of the Combustion Institute* 28 (2000) 367–373.
[29] F. Dinkelacker, A. Buschmann, M. Schafer, J. Wolfrum, *Proceedings of the Joint Meeting of the British and German Sections of the Combustion Institute*, Cambridge, UK, 1993, pp. 295–303.